Flexible picosecond probing of integrated circuits with chopped electron beams

by D. Winkler
R. Schmitt
M. Brunner
B. Lischke

The effective design and evaluation of high-speed integrated circuits is supported by internal noninvasive voltage-measurement techniques with picosecond time resolution. An electron-beam tester has therefore been developed which approaches the theoretical time-resolution limit of this method. It is based on the well-established e-beam technique for VLSI circuits, allowing for high flexibility in driving different kinds of high-frequency circuits under both conventional and critical conditions. The electron pulses of the stroboscopic test system are generated by a two-stage chopping system which was optimized to obtain very short pulses. It allows for a 7-ps effective pulse width which simultaneously yields a probe diameter of 0.5 μm and a probe current of 1 nA. This current results in a noise voltage of 20 mV when one period of a 1-GHz signal is recorded, with a total acquisition time of 0.1 s. Long-range phase shifting with high resolution is achieved by operating the upper stage of the blanking system at a high frequency and using the lower one as a selective gate. This allows propagation-delay measurements to be performed with a resolution of better than 2 ps over a range of several μs. The test system has thus far been used for the analysis of tunnel diodes, step-recovery diodes, bipolar frequency dividers, ring oscillators, and GaAs memories. Waveform measurement and evaluation at more than 60 different test points of a GaAs 1-kb SRAM in a six-hour session has demonstrated routine handling of complex high-speed circuit analysis.

Introduction

The ongoing development of high-speed integrated circuits (ICs), based on silicon as well as GaAs

technology, has led to an increased demand for internal-voltage-measurement techniques with picosecond time resolution. At the same time, the shrinking geometrical dimensions and smaller voltage swings of modern high-frequency devices require a voltage resolution in the 10-mV range and probe diameters well below 1 μm.

High-frequency circuits are being developed for a wide range of applications, from digital memories to microwave amplifiers. They have differing requirements for the signals with which they are driven during a measurement. Furthermore, thorough device testing often requires the clock frequency to be swept over a wide range. Therefore, in addition to having a high time resolution, a picosecond test system should possess highly flexible circuit-driving parameters to allow thorough checking of individual devices as well as testing of different kinds of circuits.

The electron beam is a mechanically and electrically noninvasive probe, easy to position and with high spatial and voltage resolution [1–15]. Electron-beam testing is therefore a widely accepted tool for direct voltage measurements on the interconnections of integrated circuits. Its main application has been the testing of complex VLSI and ULSI circuits, with emphasis on connection to CAD workstations and on automation to allow for high-throughput measurements of a great number of signals within a single circuit [3–5] (see the contribution by F. Fox et al. [16] in this issue).

On the basis of this well-established technique, an electron-beam tester was developed which approaches the theoretical time-resolution limits of this technique, together with high voltage and spatial resolution. It was designed to allow high flexibility in driving different kinds of high-frequency circuits [6–14].

High-frequency electron-beam testing is achieved by sampling the test signal with short electron pulses. The time resolution is given primarily by the pulse length. Because of its flexibility and the relative simplicity of the system configuration, the electron-beam tester presented in this paper was designed to generate picosecond pulses in the conventional way by chopping the electron beam with a blanking capacitor. This technique is discussed below, and its advantages, limits, and applications considered.

Operating principles

The application of e-beam testing in an industrial environment began more than fifteen years ago. Recent efforts at Siemens to develop higher speeds [6–14] have been based on the proven operating principle [1–3] which is outlined in **Figure 1**. A pulsed electron beam is focused on the point of interest within the device under test (DUT). Bombardment by primary electrons causes the probed area to emit secondary electrons (SE). A retarding grid spectrometer in front of the detector allows the secondary electrons to be analyzed with respect to their energy, thus revealing the voltage of the probed IC-internal node (voltage measurement). Synchronization between the electron pulses generated by the blanking control signal [Figure 1(a)] and the repeated signal of the DUT [Figure 1(c)] ensures that a constant voltage is sampled at a fixed phase relation. Slowly shifting the phase relation allows the waveform to be recorded [Figure 1(b)]. A feedback loop is used to keep the detector signal constant by readjusting the retarding grid of the spectrometer during the phase scan. The retarding grid voltage thus tracks the voltage of the sampled waveform and is recorded with respect to the phase shift between signal and e-beam pulses [Figure 1(b)]. The bandwidth of the detector and amplifier, including the feedback loop, can be set rather low (typically between 1 and 10 Hz), since the phase scan is slow despite recording a high-frequency signal (GHz).

Definition of time, voltage, and spatial resolutions

Before the resolution limits of the test system are discussed, these quantities must be unambiguously defined [7] (the Appendix contains a list of relevant symbols). The main characteristics for measurements in the time domain are the time resolution, which defines the error of rise-time measurements, and the phase resolution, which describes the precision of propagation-delay measurements.

Signal sampling with a gate of finite width, as is the case for chopped e-beam testing, has the effect of low-pass filtering, with the cutoff frequency depending on the sampling gate width. For sampling with a Gaussian-shaped gate of width t_g, a cutoff frequency (−6 dB attenuation) of $f_c = 0.43/t_g$ can be calculated by Fourier transform. This low-pass filtering affects the measurement of rise times. Commonly, the rise time of realistic signals is measured between the 10% and 90% amplitude values. This rise time t_s can be measured with an error of less than 25% if the sampling gate half-width t_g equals the rise time duration t_s. Further reduction of the gate width to $t_g = 0.5t_s$ results in an error of less than 10%, and $t_g = 0.2t_s$ allows measurement with an error below 1%. The effective sampling gate width thus characterizes the time resolution of the test system. It is given primarily by the electron pulse length, as is shown in the following chapters.

The term *phase resolution* refers to the attainable precision of measurements such as propagation delays and timing. It is primarily limited by the resolution with which the phase between sampling gate and signals can be shifted. The gate length, on the other hand, is of minor influence, since an increased rise time of the signal

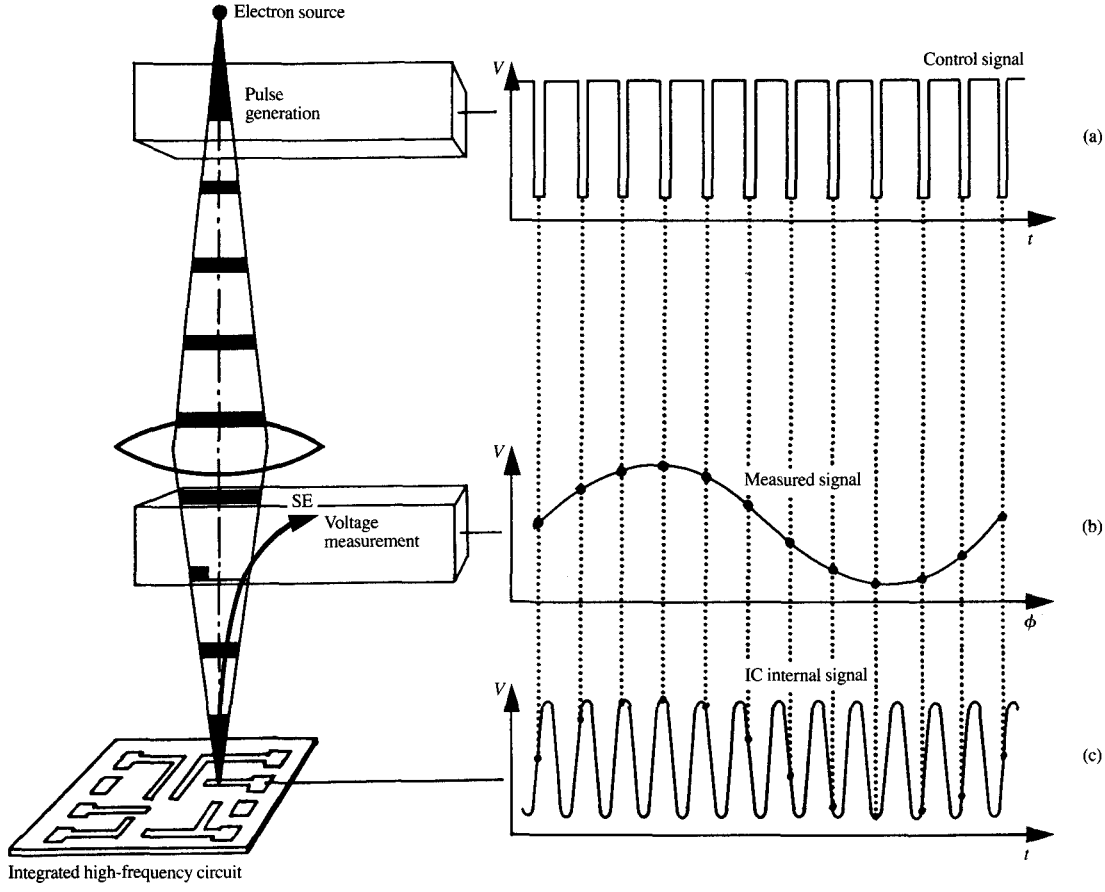

Figure 1

Principle of high-speed e-beam testing: Electron pulses (a) sample a periodic test signal (c). Slowly shifting the phase relation between the synchronized signals allows the complete waveform (b) to be recorded.

edges does not change the delay between two signals. It is assumed that the gate length remains constant during the measurement. However, a high noise voltage may also limit the phase resolution, because it influences the localization of the edges. The system phase resolution is defined as the smallest propagation delay which can be detected.

Besides the temporal resolutions, several other specifications characterize the performance of the test system. The voltage resolution of the electron-beam tester is primarily limited by the shot noise of the primary and secondary electrons. Voltage resolution is usually defined as the signal amplitude which can be recorded with a signal-to-noise ratio of 3:1. This resolution can be further degraded by microfields of neighboring potentials affecting the secondary electron energy. This error depends on the geometry of the device under test and on the secondary electron detector. On high-frequency devices, where the layout avoids signal lines in close proximity, this error is typically below 5%. Noise is thus the main limitation, and its amplitude is therefore a measure of the voltage resolution, which is the quantity to be specified.

With mechanical testers using needle probes, the spatial resolution is given by the diameter of the needle tips. Accordingly, the diameter of the electron probe which samples the signal waveforms defines the spatial resolution of the electron-beam tester. The electron beam has an approximately Gaussian intensity distribution over its diameter. To avoid signal falsification by

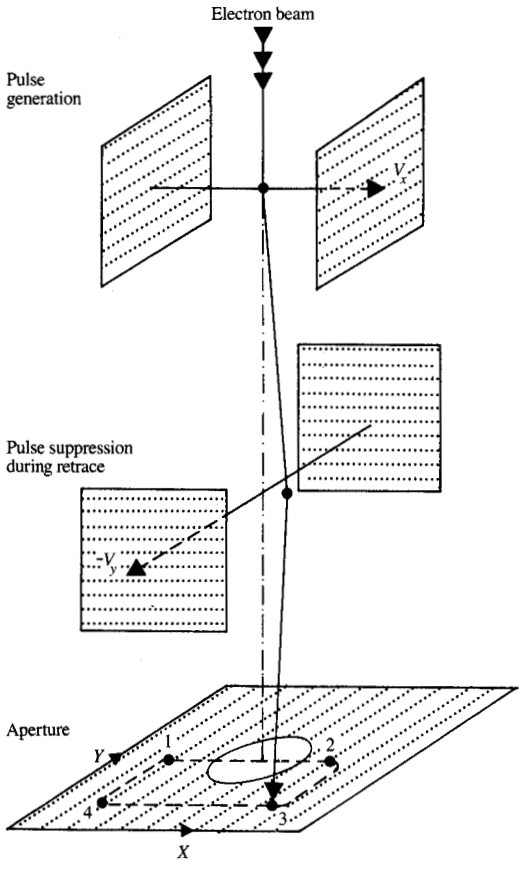

Figure 2

Pulse generation by electron-beam chopping. The electron pulses are generated by scanning the beam over an aperture with a two-stage blanking system.

electrons striking the device surface in the area surrounding the test point, and to counter instabilities of positioning, the electron-beam half-width should be about one fourth of the test point size. Beam blanking may lead to further degradation of the spatial resolution by generating a probe shift during measurement. This can be avoided by suitable design of the electron optics [10]. The effective beam diameter thus characterizes the spatial resolution.

Picosecond pulse generation and time resolution

The e-beam pulse duration is the main contribution to the effective sampling gate width which limits the time resolution [10]. In the technique discussed in this paper, the picosecond pulses are generated by beam chopping (**Figure 2**). The electron beam is scanned across an aperture by switching the voltage polarity of a capacitor situated in the beam path. The scan which is described by the electron beam in the aperture plane during one period of the clock signal is represented in the lower part of Figure 2. In the *off* state, a voltage $V_x = -V_{off}$ applied to the upper capacitor deflects the electron beam so that it does not pass the aperture (position 1). By switching this voltage to $V_x = +V_{off}$, the electron beam is scanned over the aperture into position 2, thus producing a short electron pulse. The falling edge of the driving signal from $V_x = +V_{off}$ to $V_x = -V_{off}$ would produce a second pulse during the retrace of the e-beam. To suppress this pulse, the electron beam is additionally deflected by a second capacitor (positions 3 and 4). The voltage V_y on the second capacitor is switched off again before the beginning of the next cycle (position 1). Rise and fall times of V_y thus do not influence the beam pulse width.

It seems obvious that the electron pulse width depends on the rise time of the capacitor driving voltage. However, this only holds true as long as the flight time of the electrons through the capacitor can be neglected. The effects which determine the pulse duration may be explained qualitatively. For a given rise time of the driving signal, the attained electron pulse length depends on two contradictory effects:

1. The deflection sensitivity, which is the deflection angle per volt of the control signal.
2. The electron flight time through the effective area of the capacitor.

Both effects increase with the capacitor plate length, the first one shortening the pulse duration, the second one lengthening it. The first quantity dominates at short capacitor lengths. The pulse duration decreases with increasing capacitor length up to a limit where the time of flight becomes important (**Figure 3**). A lower limit for the pulse duration is reached when the electron flight time t_f through the capacitor equals the sum of capacitor voltage rise time t_r and electron pulse width t_p ($t_f = t_r + t_p$). Operating at this limit makes the pulse duration independent of the rise time of the driving signal, and the flight time t_f varies with the capacitor length.

A quantitative analysis [10] yields an equation for the minimum pulse width,

$$t_p = \left(\frac{2m_e V_p}{e}\right)^{1/2} \left(\frac{h\alpha_b}{V_{off}}\right), \quad (1)$$

where V_p is the primary electron voltage, h is the spacing of the capacitor plates, V_{off} is the amplitude of the capacitor voltage signal, and α_b is the deflection angle required to switch the beam on and off again.

In the practical case which has been realized in the Siemens tester (V_p = 2.25 kV, h = 400 μm, $\alpha_b = 3 \times 10^{-4}$ rad, and V_{off} = 10 V), the minimum pulse length has a theoretical value of 2 ps (Figure 3). It is independent of the capacitor-voltage rise time. A further increase in the capacitor length does not lead to further electron pulse reduction, but it allows driving signals with longer rise times to be used. However, a long capacitor-voltage rise time limits the pulse-repetition rate. The capacitor voltage must remain at its maximum value for a time at least equaling the electron pulse length t_p to achieve maximum deflection sensitivity. The maximum repetition rate is thus $f_r = 2(t_r + t_p)^{-1}$. A 80-ps rise time results in a maximum repetition frequency of 6 GHz. This limitation applies to the generation of the electron pulses only. Signals of higher repetition rates can still be measured by choosing a sampling frequency which is a fraction of the signal clock rate.

The 2-ps pulses produced by the chopping system are degraded on their way to the test point by the dispersion due to the energy width of the electron beam. The energy spread of the LaB_6 electron gun was measured to be 1.25 eV at 2.25-keV acceleration voltage. The resulting velocity spread theoretically leads to a pulse width of t_d = 3 ps in view of the 30-cm distance between the chopping system and the device under test. This shows that a further optimization of the electron-beam chopping system alone would not result in shorter probing pulses.

Besides the pulse duration, there is an important effect limiting the sampling gate width. This is the jitter in the timing between the pulse generation and the signal to be measured on the chip, which causes an effective broadening of the sampling gate. The jitter was measured to be approximately t_j = 5 ps in the present setup. In summary, the effective gate width t_g can thus be expressed by the square sum $t_g = (t_p^2 + t_d^2 + t_j^2)^{1/2}$. The effect of the transit time of the secondary electrons on the sampling gate width is treated later.

The electron pulse width including broadening by jitter was measured directly using a streak-camera method [2] with a calculated time resolution of 3 ps. The measured pulse is shown in **Figure 4**. Its half-width of 7 ps includes the time resolution of the streak camera itself. The effective gate length which determines the time resolution is given primarily by this pulse width, but further degradation may occur due to the transit-time effect, which is discussed later.

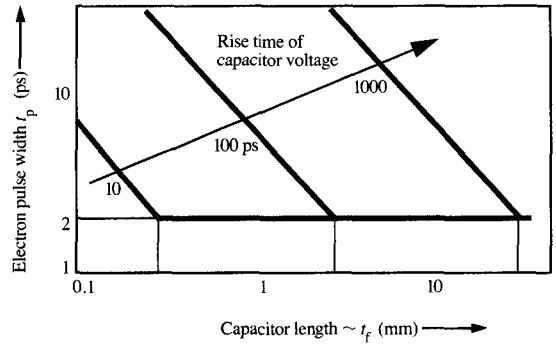

Figure 3

Electron pulse width as a function of capacitor length. The minimum pulse width is independent of the capacitor plate length. It is determined by the capacitor voltage amplitude and the deflection sensitivity of the electron-optical system. Large capacitor lengths allow for long capacitor-voltage rise times.

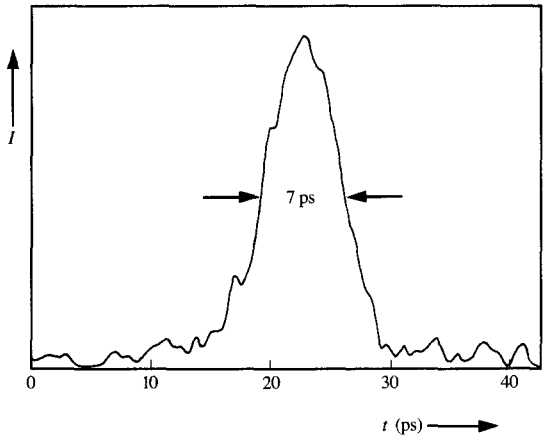

Figure 4

Shape of the 7-ps electron pulses generated by the picosecond e-beam tester.

Acquisition-time, spatial, and voltage resolution

The ultimate values of spatial, voltage, and time resolution allowing a signal to be recorded within a specific acquisition time are related to one another [7]. The time resolution has been defined above by the effective sampling gate width. Spatial and voltage resolutions are related respectively to the beam diameter and the noise voltage. The relationship between these values is explained by first considering the electron pulse, which is schematically represented with a rectangular shape in **Figure 5**. The current at the probed point is I_0 during the pulse and zero at all other times. The height of the rectangular pulse, which is the probe current I_0, is

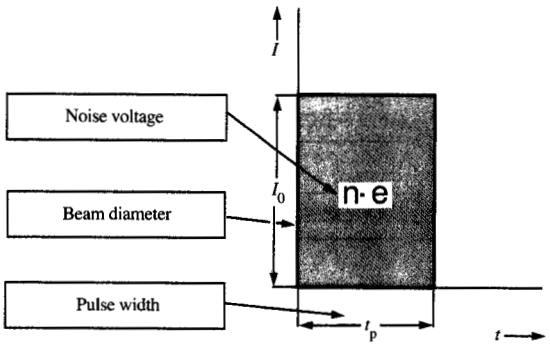

Figure 5

Schematic representation of a rectangular electron pulse showing the relationship among noise voltage, beam diameter, and pulse width. The pulse width defines the time resolution. Its height is proportional to the beam diameter, while its area is inversely proportional to the noise voltage.

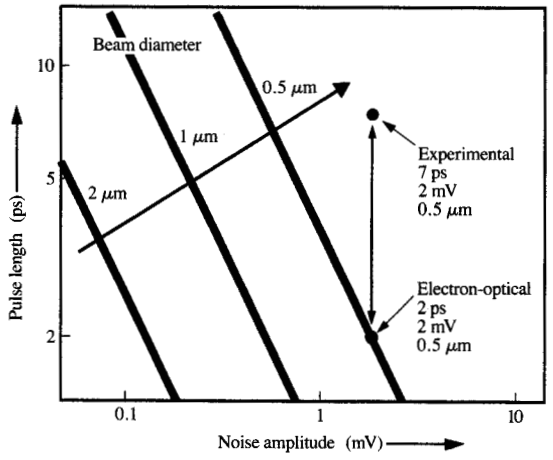

Figure 6

Relationship of pulse width, beam diameter, and noise voltage. Jitter and pulse dispersion shift the value of 2 ps, which is expected from electron-optical considerations, to the measured value of 7 ps (repetition frequency $f_r = 1$ GHz, interval length vs. acquisition time $t_s/t_a = 3.3 \times 10^{-11}$, electron-optical constant $C = 5.5 \times 10^{-18}$ V-m^2-s$^{1/2}$).

related to the beam diameter and thus to the spatial resolution via the electron-optical properties of the electron-optical system. The width is the pulse duration t_p, which determines the time resolution. The area under the curve gives the number of electrons available per pulse, which corresponds to the shot-noise level ultimately limiting the attainable voltage resolution.

The height and width of the electron pulse should be as small as possible to achieve good spatial and time resolution, while the hatched area should be as large as possible for a low noise level. A low noise level can also be attained by integrating over a large number of pulses. This, however, increases the acquisition time t_a. A compromise must be made for each measurement to meet the specific requirements.

The relationship among beam diameter, noise voltage, and electron pulse width has been calculated in detail as a function of the measuring systems' cutoff frequency [7], taking into account the spherical and chromatic aberrations of the system. This relationship can be simplified by expressing the cutoff frequency as a function of the electron pulse width t_p: In compliance with customary definitions, the cutoff frequency is defined as the value at which the measured signal is attenuated by 6 dB. For sampling with a Gaussian-shaped pulse this condition is fulfilled for $t_p = 0.43/f_c$. Further simplifications result from consideration of only the chromatic aberrations, which primarily define the minimum beam diameter at the usual operating conditions. An optimum aperture can thus be calculated as a function of beam diameter and chromatic error to obtain maximum current together with minimum spot size. The minimum pulse width which results with these assumptions is expressed by

$$t_p = C\left(\frac{1}{d^2}\right)\left(\frac{1}{V_n}\right)\left[\left(\frac{t_l}{t_a}\right)\left(\frac{1}{f_r}\right)\right]^{1/2}, \qquad (2)$$

where C is a constant which describes the electron-optical quality of the system, t_l/t_a is the length t_l of the signal to be recorded in relation to the time t_a, f_r is the pulse-repetition frequency, V_n is the noise voltage, and d is the electron-beam diameter. **Figure 6** shows the application of this formula to the parameters of the Siemens electron-beam tester. [A value for the electron-optical constant of $C = 5.5 \times 10^{-18}$ V-m^2-s$^{1/2}$ results for a primary beam voltage $V_p = 2.25$ kV, energy width $E_w = 1.25$ eV, chromatic aberration constant $C_c = 15$ mm, spectrometer constant $C_s = 6.3 \times 10^{-9}$ V(A-s)$^{1/2}$, and detector noise factor $C_d = 4$.] It shows that under the given conditions, a pulse width of 2 ps is expected at a noise amplitude of 20 mV and a beam diameter of 0.5 μm, for a value of $t_l/t_a = 3.3 \times 10^{-11}$ and at a repetition frequency of 10 MHz. The optimal beam aperture in this case is $\alpha = 3 \times 10^{-2}$ rad.

Typical waveforms to be sampled with picosecond pulses are usually not recorded over a range larger than

several nanoseconds. At longer ranges, the high time resolution is not necessary because it cannot be represented in the printout. A larger sampling-gate width can be used in this case. With $t_l/t_a = 3.3 \times 10^{-11}$, a 1-ns interval of a 10-MHz signal is sampled with a beam of 0.5-μm spot size during 30 s of acquisition time, yielding 20 mV of noise. The probe current is 1 nA. For a 1-GHz repetition rate signal, the measuring time reduces to $t_a = 0.3$ s with the same spatial, voltage, and time resolutions.

The above calculations represent the ultimate limits of this technique. They do not include dispersion and jitter, which in this case increases the pulse width from 2 ps to 7 ps. This is the pulse width which was measured together with a beam diameter of 0.5 μm and a noise level of 20 mV at a repetition frequency of 10 MHz (Figure 6).

A smaller beam diameter (down to 0.3 μm) is obtained for 40-mV voltage resolution and the values given above. Further improvements of the spatial resolution require optimization of the electron-optical column, such as shielding the electron beam against magnetic stray fields.

Phase resolution and long-range phase shift

The phase resolution is the limiting factor for propagation-delay measurements. In principle it also influences rise-time measurements, but in practice the effect is negligible compared with the influence of the electron pulse width. A high-resolution phase shift with a small range can be realized using a transmission line of variable length (trombone line stretcher). **Figure 7** shows a pulse of a step-recovery diode on a coplanar strip line. The delay caused by the signal propagation along this line was measured using this mechanical phase-shift device. A 3.5-ps delay can easily be resolved, and values below 2 ps seem to be detectable. From the measured 38-ps rise time, a real signal slope of 35-ps duration can be deduced by deconvolution with the 7-ps pulse.

Unfortunately, mechanical delay lines are limited to delays of less than a few nanoseconds. A mechanical delay line for a 100-μs phase shift, for example, would require a variable length of 30 m. Losses and dispersion over this length would be much too high for stable operation. Electronic delay devices such as digital delay lines cover large delay ranges but have limited accuracy and stability. Jitter is typically of the order of several tens of picoseconds. To allow for long-range phase shifts with high accuracy and stability, a phase-shift method has been developed by controlling the two-stage blanking system of the e-beam tester in a suitable way [11]. The operating principle is shown in **Figure 8**. The first capacitor, driven by V_x, produces short electron pulses with a repetition rate of, say, 1 GHz by sweeping the beam across an aperture. The second capacitor in the

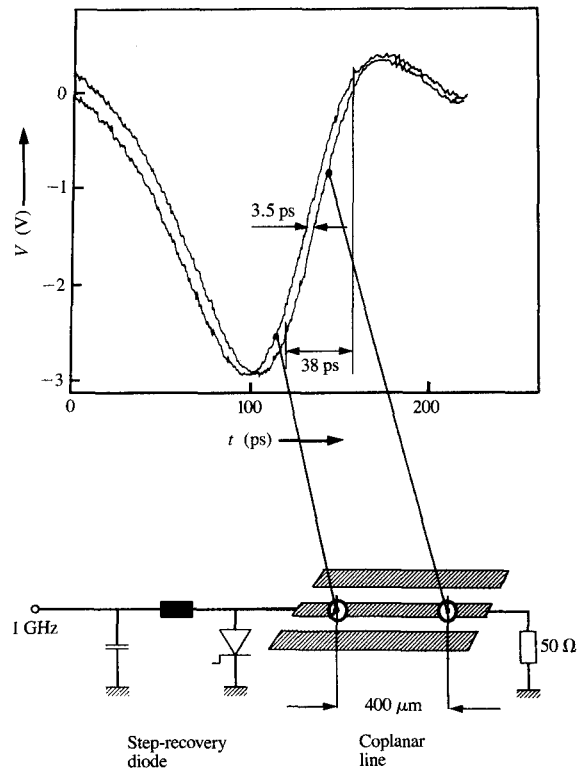

Figure 7

Signal of a step-recovery diode sampled by e-beam on a coplanar line. A propagation delay of 3.5 ps between two probed points is resolved and agrees with the expected theoretical values.

beam path, driven by V_y, acts as a gate which selects appropriate pulses to match the clock rate of the signal to be measured (e.g., 10 MHz). Additionally, the pulse selection determines the phase point of the probed signal. As shown in Figure 8, the position of the sampling pulse on the time axis is given by the position of the gate V_y. It can be shifted by one period of V_x if the gate V_y is shifted by approximately the same value. In this way, a coarse position of the phase relation between the e-beam pulses and the signal to be measured can be selected. The superimposed continuous fine delay, which is necessary to record a waveform, is generated by a mechanical delay unit. Another way of performing this short-range delay is the phase shift by electron-beam deceleration, which was presented by Thong et al. [17]. The advantage of the long phase-shift technique presented here is that the control signal V_y driving the pulse-selecting capacitor can be realized with low stability over a range of several microseconds using electronic delay lines. As long as the

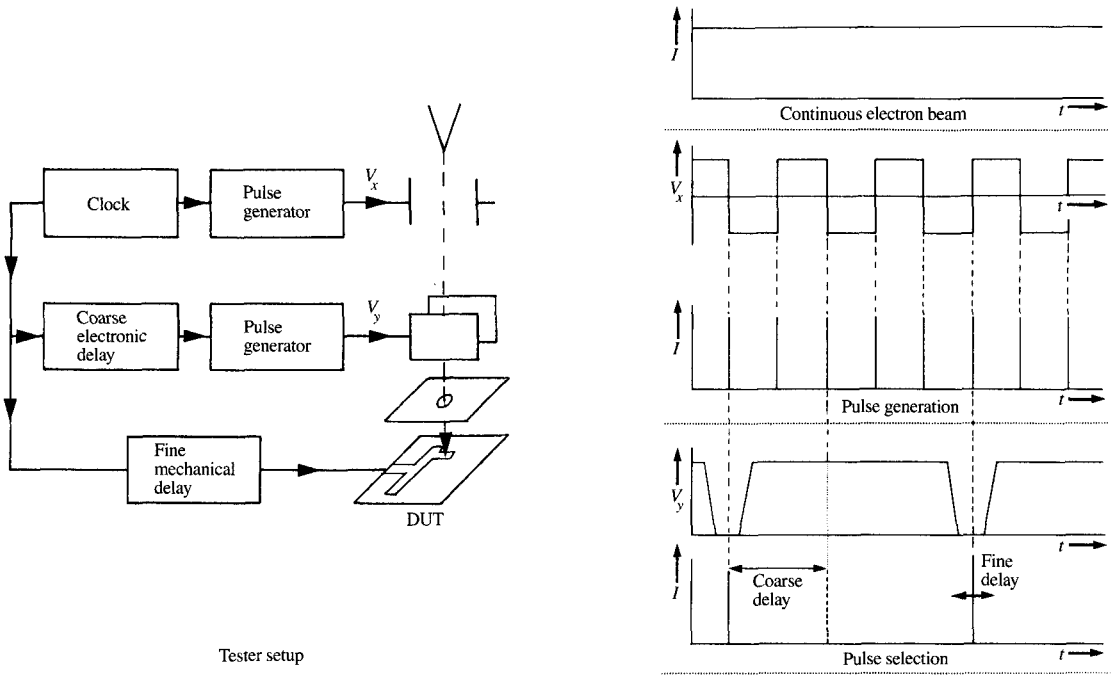

Figure 8

Principle of the long-range phase-shift method. A capacitor driven by V_y with the repetition rate of the device under test selects the phase of the short electron pulses produced by the capacitor V_x.

position of the selecting gate varies less than its width, it still selects the same pulse from the 1-GHz signal. The stability is thus determined only by the precision of the initial pulse generation and the quality of the fine-delay unit. These, however, can be realized with an accuracy of a few picoseconds.

This phase-shift technique has an additional advantage. The pulse-generating capacitor can be switched off, leaving only the second capacitor active. This capacitor, however, generates electron pulses of long duration. Broad pulses result in a good signal-to-noise ratio, which in turn leads to short recording times. The pulse duration is determined by the time in which the control voltage V_y is zero, and can thus be adjusted. Continuously shifting the coarse delay gives a fast overview of the measured signal with a reduced time resolution.

Figure 9 shows the output signal of a tunnel diode with a 10-MHz repetition frequency which was measured using this technique. The overview was recorded in the way just described. The phase was shifted with the electronic delay. A 100-ns period of the signal required 10 s of total acquisition time. Stopping this shift at a section of interest and switching on the upper capacitor allows this section to be measured with high time resolution by shifting the phase with the mechanical delay line. The time correlation with the previous measurement is retained. The acquisition time for this 200-ps interval was 50 s (note the small-signal amplitude of 150 mV). The noise voltage is about 5 mV for both waveforms. An electron-beam spot size of 0.5 μm was used.

Transit-time effect

The transit-time effect is caused by the change of the potential field above the device surface associated with the alternating signal at the test point. This effect has been discussed in detail by Fujioka et al. [18] and Clauberg [19] and is treated here qualitatively together with experimental results [14]. At the time of emission, the secondary electrons have a potential energy $eV_s(t)$ given by the test-point voltage $V_s(t)$. They are accelerated toward the spectrometer; before they enter the retarding

field spectrometer, their potential energy has been converted into kinetic energy. Their total energy remains unchanged throughout this process, if a constant field is considered. The energy of the secondary electrons reveals the test-point voltage without any error in this case.

This description is no longer valid if the potential changes while the electron is still close to the point of emission, which is the typical situation at very high frequencies. In this case, the secondary-electron energy reveals the average of the potential during the time the electron spends in the electrical field of the test point. This time is determined by the speed of the secondary electrons and the spatial extent of the electrical field, the latter depending on the test-point dimensions. The electrical field of a large test point extends further above the surface than the electrical field of a smaller electrode. In an approximation, the transit-time effect causes an effective broadening of the sampling gate t_g by a value t_t, where t_t is the flight time of the secondary electrons through the electrical field of the test point: $t_g^2 = (t_p^2 + t_d^2 + t_j^2) + t_t^2$ [14]. This broadening is not symmetrical with respect to the time t of emission from the surface. It extends from t to $(t + t_t)$. This asymmetry leads to a time shift and an attenuation of the measured signal, which does not, however, lead to errors if the electrons are affected equally at different test points. Different geometries of the probed points, on the other hand, lead to different transit times, which may cause errors in propagation delay measurements (see **Figure 10**).

The transit-time effect can be estimated [14] on the basis of the calculations of Fujioka et al. [18]. On a test point of width and spacing of $w = 10$ μm with a resulting extension of the electrical field of 40 μm, an initial electron energy of 3 eV and an accelerating field of 3 kV/mm result in a transit time of $t_t = 10$ ps. This reduces to $t_t = 3$ ps on 1-μm width and spacing. For the high-speed e-beam tester, the 10-ps transit time leads to a widening of the effective sampling gate from 7 ps to 12 ps, while the effect of the 3-ps transit time can be neglected.

The transit-time effect was investigated experimentally by feeding a 12-GHz signal to a coplanar strip line with variable width. The line width was equal to the spacing between signal and ground lines at all points. **Figure 11** shows the waveforms measured at different line locations. The signal propagation delays between these points were negligibly small (<0.5 ps between adjacent test points), so the shifts of the measured waveforms can be fully attributed to the transit-time effect. The broadening of the gate due to the transit-time effect leads to an

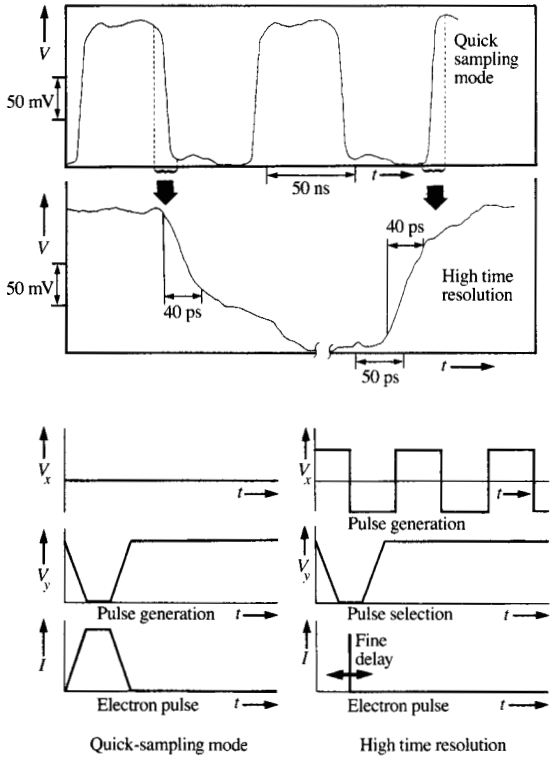

Figure 9

Quick-sampling mode and high-resolution mode of the long-range phase-shift method. Waveform measurement of a tunnel diode pulse using this technique.

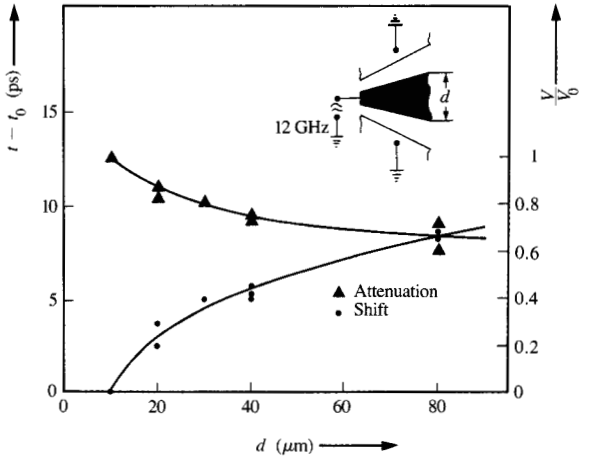

Figure 10

Phase shift and attenuation of a measured sine wave due to the transit-time effect as a function of line width d. Reference is made to a line width of 10 μm corresponding to t_0, V_0.

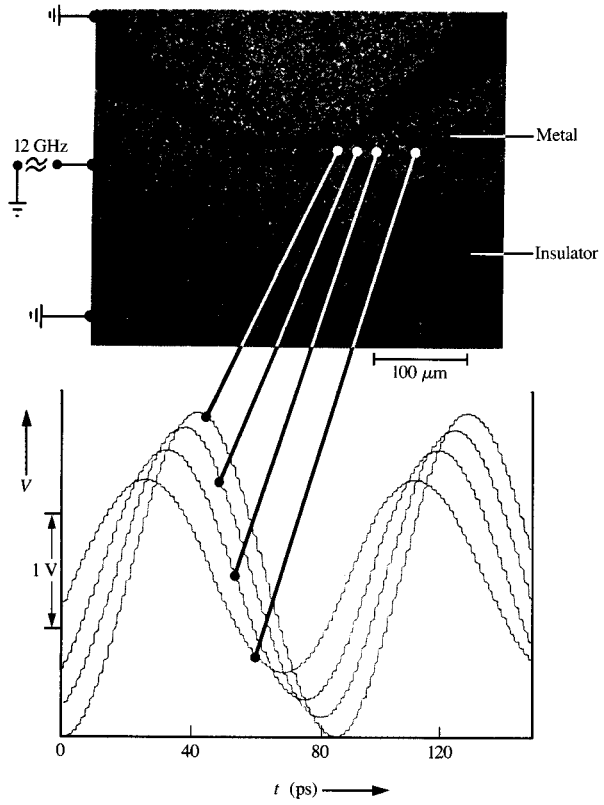

Figure 11

Waveforms of a 12-GHz signal recorded on different line widths. The measured signal attenuation and the observed phase shift between adjacent test points of more than 5 ps are due to the transit-time effect. (The propagation delay between test points is less than 0.5 ps.)

attenuation of the signal amplitude with an increasing line width w and thus increasing transit time t_t due to more extended fields. Additionally, the measured waveforms are shifted with increasing line width w. Figure 10 shows the shift on the time scale, taking the measurement on the 10-μm width as a reference. For example, the measured signal on a 20-μm conductor is shifted by $(t - t_0) = 3$ ps relative to a waveform recorded on a 10-μm-wide line. The signal attenuation, compared with the amplitude V_0 at $w = 10$ μm, is also shown in Figure 10.

The transit-time effect is the factor which ultimately limits the time resolution. However, for the conditions encountered in the testing of high-speed integrated circuits, test points with dimensions below 5 μm still allow a resolution of better than 4 ps.

Noninvasiveness

Mechanical probes introduce a capacitive and ohmic load to the device under test. This changes the device operation, especially at high speeds, and thus limits mechanical probing to certain applications. It is important to know how the electron-beam technique compares in this respect. The yield of secondary-electron emission upon impact of the electron probe depends on the energy of the primary beam. At two values of primary energy the yield is unity, the lower value being typically in the range of 100 eV and the higher value in the range of 1 keV and above. These values depend on the material and surface conditions of the probed point. A nonloading operation of the e-beam tester can therefore be achieved by selecting the probing beam energy at one of these values, to produce compensation of primary and secondary currents. However, in most cases this energy causes charging of the substrate. On silicon devices, operation at approximately 1 keV is commonly accepted as a compromise. On GaAs circuits containing gold wiring, compensation at the probed location on the line would require operation at 9 keV. In this case, an energy in the range between 1 keV and 2.5 keV is used for minimum charging. Although the secondary and primary currents partially compensate, this is not a true nonloading condition. On average, however, probing with very short pulses causes less than one electron to strike the device during one cycle. Therefore, any influence on the device function is also avoided in this case.

Although radiation damage and trapping of charges are possible in principle, these effects are negligible at low primary energies in the neighborhood of 1 keV [2]. In order to verify this noninvasiveness on GaAs devices, the leakage currents of GaAs depletion-mode MESFET transistors were measured before, during, and after electron irradiation. No influence was observed with the pulsed beam. A continuous beam, which is not used in practice for testing, caused a leakage current of the order of the beam current when focused on the gate. However, the transistor data remained the same before and after this heavy exposure.

Summarizing, it can be stated that the e-beam does not influence the device function, either during or after the test, and thus is noninvasive.

Control and synchronization

In the following, the application of e-beam testing to electronic high-speed devices with a large variety of operating conditions is described.

The electron-beam tester permits measurements to be made on devices independently of their substrate material. For example, silicon-based as well as GaAs circuits can be tested. The present system has thus far been used only for measurements on unpassivated surfaces. However, in principle test spots covered by passivation layers can also be tested [20, 21].

The primary applications for the picosecond electron-beam tester are waveform and propagation-delay measurements. However, in addition to conventional test systems, the picosecond electron-beam tester allows for test methods such as voltage coding and logic-state mapping [1].

Addressing different spots on a single chip or different chips on a wafer is performed by computer-controlled driving of the prober stage. Finding a new test spot thus takes only a few seconds. Currently, the test-point data lists must still be implemented manually, as no link to CAD data is provided.

The picosecond electron-beam tester allows for flexible operation of different kinds of high-frequency circuits. The synchronization between the electron pulses and the signal to be sampled can be achieved in different ways, depending on the application. Since most circuits are designed to be operated with an external clock, the most common operation mode uses the clock signal, which also synchronizes the electron pulses to trigger the device (e.g., Figure 14, shown later). If signals in the circuit with repetition rates lower than the clock frequency are to be measured, the DUT and the electron beam are both controlled by external generators at different but synchronized frequencies. The same setup is used if the circuit is to be operated with frequencies which are higher than the maximum repetition rate of the electron pulses. The electron-pulse frequency is then chosen to be a fraction of the signal-repetition frequency. The maximum signal frequency is thus not limited by the test method. Furthermore, it can be continuously swept, thus enabling device parameters to be tested in dependence on the clock frequency (e.g., Figure 12, shown later). The device can be operated with any input signals such as pulses, logic signals, and sine waves.

Some circuits cannot be synchronized to an external signal. Even so, free-running devices such as ring oscillators can be measured by synchronizing the electron beam to an output signal (e.g., Figure 13, shown later). Even long-term fluctuations of the device frequency due to, say, thermal effects do not present a problem, as the test system remains locked to the device signal.

Measurements may be performed on packaged circuits, provided the chip surface is not covered. Tests can also be performed on chips on high-frequency microstrip mounts. On-wafer measurements become possible by combining the electron-beam tester with a wafer prober which was designed to suit the special geometrical requirements [12]. Operating the electron-beam tester in the SEM mode allows the prober to be positioned easily on the pads.

At frequencies approaching several GHz, the trigger signal which is supplied to the device under test may be attenuated and slightly distorted due to imperfect

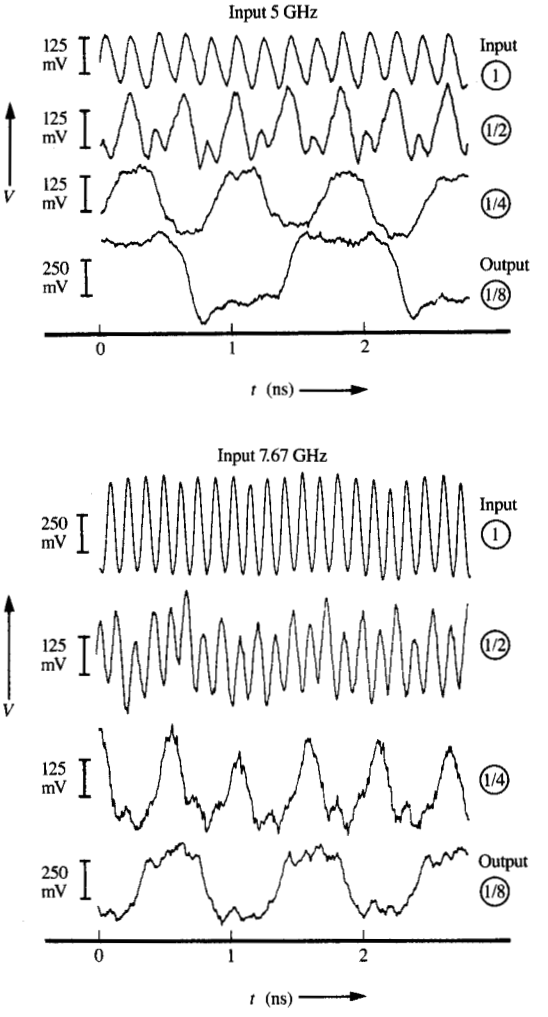

Figure 12

E-beam-probed internal signals of a silicon 8:1 frequency divider. Overshooting causes malfunction at frequencies above 7.67 GHz.

impedance matching of the vacuum feed-throughs and the wafer prober itself. However, the electron-beam prober is used in this case to control *in situ* the input signal supplied by the prober. For example, a sinusoidal 12-GHz signal was fed to a chip input via the prober. Although attenuation by the prober reduced the 16-V peak to 2.6 V at the IC pad, the amplitude was still high enough to serve as a fast input signal. The signal amplitude and shape could be controlled by measuring the actual waveform with the e-beam.

When performing measurements on packaged or bonded chips, where no wafer prober is needed, the maximum trigger frequency depends on the vacuum feed-through. Commercial feed-throughs have cutoff

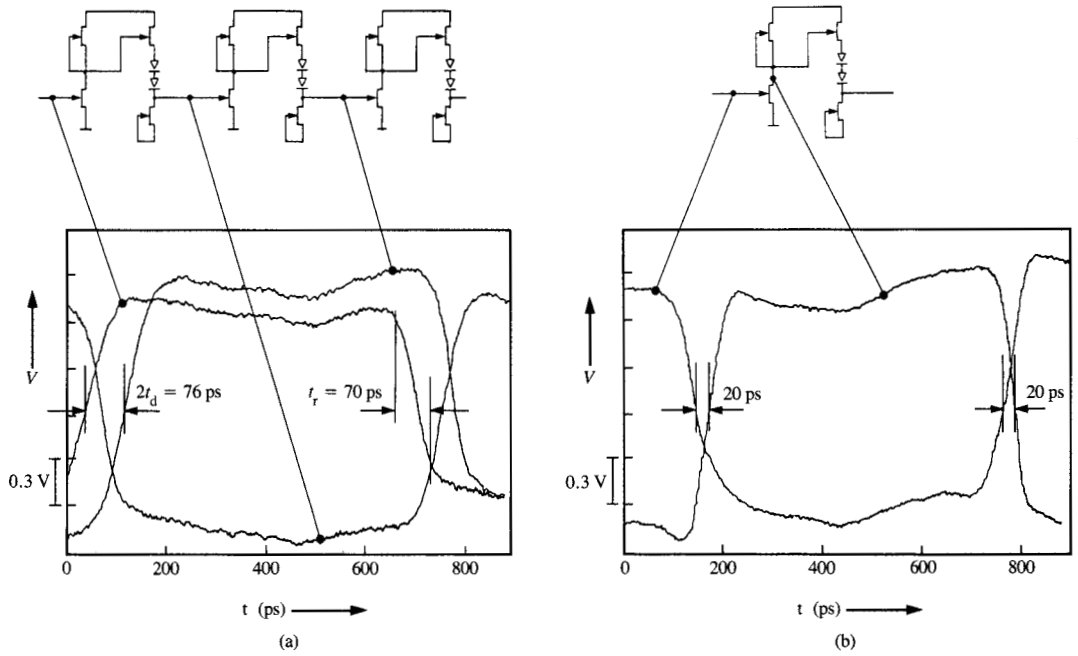

Figure 13

Internal waveforms of a GaAs ring oscillator measured directly on the wafer: (a) Variations of gate delays t_d, signal rise times t_r, and voltage levels. (b) Determination of the switching speeds of individual transistors.

frequencies of 18 GHz. However, losses and distortions at higher frequencies can be compensated by *in situ* inspection of the clock signal directly on the chip as described above. This allows for measurements at considerably higher frequencies.

The following section presents some practical results in which advantage was taken of the flexibility of device operation.

Device characterization

Figure 12 shows internal waveforms of a static silicon bipolar 8:1 frequency divider IC [22] measured by the e-beam system. The clock signal was supplied by an external source. The circuit output signal, having 1/8 of the input frequency, was used to synchronize the electron pulses. The signals at the different divider stages could be viewed directly, and changes with input frequency were observed. Overshooting at the first divider stage increased with increasing input frequency, causing malfunction of the device at 7.67 GHz. The e-beam system allowed the IC to be operated under its normal conditions and to continuously sweep the input frequency. The chip was bonded to a ceramic substrate to supply power and the input signal.

GaAs ring oscillators were characterized directly on-wafer, by using the wafer prober to provide the supply voltages. The output of the free-running oscillators was used to synchronize the electron-beam tester. They were evaluated with respect to rise time, voltage swing, and delay of single transistors [23] (**Figure 13**). The gate delay of t_d = 38 ps agrees very well with the oscillator frequency. It was found that the spread of individual gate delays within a ring oscillator is approximately the same as that deducible from the oscillator frequencies over the whole wafer. This indicates that the process variations causing these different delays are of a short-range type, rather than being systematic long-range nonreproducibilities. The measurement on an individual switching transistor of a gate demonstrates that it causes only about half of the total gate delay.

Circuit analysis: Timing and waveforms

Measurements on a 1-kb GaAs SRAM are presented as an example of a more complex circuit and its analysis [24]. The goal was to compare the measured signals with the simulated data. The circuit was triggered by applying an external clock which was synchronized to the electron pulses. **Figure 14** shows a comparison of the simulated

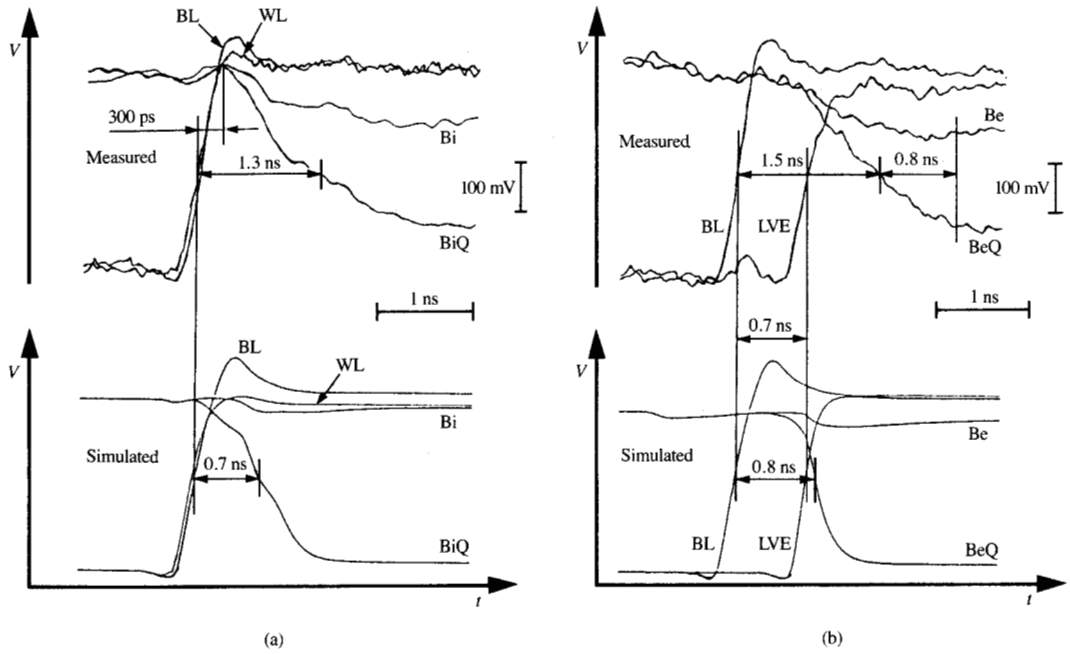

Figure 14

Comparison of simulated signals with waveforms measured by electron beam: Analysis of the address buffer of a GaAs 1-kb SRAM: (a) internal bit lines; (b) external bit lines.

and measured bit-line response of a memory cell. It can be seen that the internal bit-line potentials BI and BIQ separate later than in the simulation [Figure 14(a)]. This is an indication of capacitive coupling between the bit lines. Figure 14(b) shows the measured signals of the external bit lines BE and BEQ. The observable level degradation of BE in comparison to the simulated data is attributed to the insufficient driving capability of the external sense amplifier.

The accurate comparison between measured and simulated waveforms gave access to direct evaluation of parasitic capacitance loads as well as inaccuracies of the simulation program, allowing a more rapid and precise redesign. The long-term stability was excellent and did not require readjustment. It was possible to determine timing delays with an accuracy of less than 20 ps between signals which were measured at the beginning and at the end of a six-hour session. Waveform measurement and evaluation of more than 60 different test points in this time demonstrated routine handling of complex high-speed circuit analysis.

Conclusions

Electron-beam testing, which is a well-established technique in VLSI diagnosis, has also demonstrated its capacity for testing in the picosecond time scale. The 7-ps effective sampling pulse width of the e-beam tester currently allows the evaluation of high-frequency devices with 0.5-μm probe diameter and 2-mV/$\sqrt{\text{Hz}}$ noise voltage at 1-GHz repetition frequency. A beam diameter of 0.3 μm is attainable for 4-mV/$\sqrt{\text{Hz}}$ noise voltage. Further improvements of the spatial resolution require optimization of the electron-optical column, such as improved shielding. Low noise measurements with short acquisition times are possible.

Because of its flexibility in the selection of operation parameters for different kinds of circuits and its applicability independent of the substrate material, e-beam testing is well suited to sustain the development and analysis of current and next-generation high-speed electronics.

Appendix: List of symbols

C = electron-optical constant
C_c = chromatic aberration constant
C_d = detector noise factor
C_s = spectrometer constant
E_w = electron-beam energy width
I_0 = probe current
V_n = noise voltage

V_{off} = capacitor voltage amplitude
V_p = primary electron voltage
V_s = test-point voltage
V_x = capacitor voltage
V_y = capacitor voltage
d = electron-beam diameter
e = elemental charge
f_c = cutoff frequency
f_r = repetition frequency
h = spacing of the capacitor plates
m_e = electron mass
t_a = acquisition time
t_d = gate width due to velocity spread
t_f = electron flight time through the capacitor
t_g = effective gate width
t_j = gate width due to electronic jitter
t_l = signal length
t_p = electron pulse width
t_r = capacitor-voltage rise time
t_s = signal rise time
t_t = transit time
w = line width
α_b = deflection angle

References

1. H. P. Feuerbaum, "Electron-Beam Testing: Methods and Applications," *Scanning* **5,** 14–24 (1983).
2. E. Menzel and E. Kubalek, "Fundamentals of Electron Beam Testing of Integrated Circuits," *Scanning* **5,** 103–122 (1983).
3. H. Rehme, Elektronenstrahl-Potentialmesstechnik. *Mess- und Prüftechnik,* M. Zerbst, Ed., Springer-Verlag, Munich, 1986.
4. K. Ura, "Electron Beam Testing in Electronics," *Proceedings of the XIth International Congress on Electron Microscopy,* Vol. I, Kyoto, Japan, 1986, pp. 173–176.
5. E. Wolfgang, "Electron Beam Testing," *Microelectron. Eng.* **4,** 77–106 (1986).
6. R. Schmitt, D. Winkler, and B. Lischke, "E-Beam Testing of High-Speed Devices," *Microelectron. Eng.* **5,** 523–530 (1986).
7. B. Lischke, D. Winkler, and R. Schmitt, "The Limits of High-Speed E-Beam Testing," *Microelectron. Eng.* **7,** 21–39 (1987).
8. M. Brunner, D. Winkler, R. Schmitt, and B. Lischke, "Electron-Beam Test System for High-Speed Devices," *Scanning* **9,** 201–204 (1987).
9. R. Schmitt, D. Winkler, M. Brunner, and B. Lischke, "Electron Beam Sampling of IC-Internal GHz Signals," *Electron. Lett.* **24,** 235–236 (1988).
10. D. Winkler, R. Schmitt, M. Brunner, and B. Lischke, "Pulstastsystem für die Elektronenstrahlmesstechnik im Pikosekundenbereich," *Optik* **78,** 165–172 (1988).
11. D. Winkler, R. Schmitt, M. Brunner, and B. Lischke, "A Stable Phase-Shift Technique for E-Beam Testing with ps Time Resolution," *Scanning* **11,** 100–103 (1989).
12. R. Schmitt, D. Winkler, M. Brunner, and B. Lischke, "A GHz Wafer Prober for E-Beam Testing in a ps Time Scale," *Microelectron. Eng.*, in press.
13. M. Brunner, R. Schmitt, D. Winkler, and B. Lischke, "Noninvasive Waveform Measurements of IC Internal Signals in a ps Time Scale," *Microelectron. Eng.* **9,** 405–410 (1988).
14. D. Winkler, R. Schmitt, M. Brunner, and B. Lischke, "The Influence of the Transit Time Effect on Propagation Delay Measurements by Electron and Photon Beam Sampling Techniques," *Microelectron. Eng.* **9,** 453–456 (1988).
15. P. May, J.-M. Halbout, and G. Chiu, "Picosecond Photoelectron Scanning Electron Microscope for Noncontact Testing of Integrated Circuits," *Appl. Phys. Lett.* **51,** 145–147 (1987).
16. F. Fox, J. Kölzer, J. Otto, and E. Plies, "A Submicron Electron-Beam Tester for VLSI Circuits Beyond the 4-Mb DRAM," *IBM J. Res. Develop.* **34,** 215–226 (1990, this issue).
17. J. T. L. Thong, B. C. Breton, and W. C. Nixon, "High-Speed Electron Beam Testing Using an Electron-Optical Phase-Shift Element," *Electron. Lett.* **24,** 1441–1442 (1988).
18. H. Fujioka, K. Nakamae, and K. Ura, "Analysis of the Transit Time Effect of the Stroboscopic Voltage Contrast in the Scanning Electron Microscope," *J. Phys. D.: Appl. Phys.* **18,** 1019–1027 (1985).
19. R. Clauberg, "Microfields in Stroboscopic Voltage Instruments via Electron Emission," *J. Appl. Phys.* **62,** 1553–1559 (1987).
20. Y. Watanabe, Y. Fukuda, and T. Jinno, "SEM Voltage Contrast Mechanism of Passivated Devices," *Appl. Phys.* **24,** 1294–1297 (1985).
21. S. Görlich, K. D. Herrmann, W. Reiners, and E. Kubalek, "Capacitive Coupling Voltage Contrast," *Scanning Electron Microscopy,* Part 2, 447–464 (1986).
22. P. Weger, L. Treitinger, R. Reimann, and H.-M. Rein, "Static 7-GHz Frequency Divider IC Based on a 2-μm Si Bipolar Technology," *Electron. Lett.* **23,** 192–193 (1987).
23. T. Grave, R. Schmitt, D. Winkler, K. Anger, J. Hoepfner, H. J. Siweris, J. E. Müller, and W. Kellner, "GaAs-Submicron Ring Oscillators Characterized by Electron Beam Testing," *Proceedings of the 1988 GaAs Integrated Circuit Symposium,* Nashville, TN, 1988, pp. 209–212.
24. D. Winkler, R. Schmitt, M. Brunner, and J. M. Dortu, "On-Wafer Picosecond E-Beam Testing Applied to Complex High-Speed IC's, *Proceedings of the Microcircuit Engineering Conference,* Cambridge, 1989.

Received April 28, 1989; accepted for publication August 3, 1989

Dieter Winkler *Siemens Research Laboratories, Otto Hahn Ring 6, D8000 Munich, Federal Republic of Germany.* Dr. Winkler received his diploma in electrical engineering at the Aachen Technical University in 1984 and his Ph.D. from the University of Tübingen, FRG, in 1988. His Ph.D. thesis centered on the development of a high-speed electron-beam test system for integrated circuits and was done at the Siemens Research Laboratories in Munich. In 1987 Dr. Winkler joined Siemens, where he is currently engaged in research and development in the area of electron-beam techniques.

Reinhold Schmitt *Siemens Research Labortories, Otto Hahn Ring 6, D8000 Munich, Federal Republic of Germany.* Mr. Schmitt was awarded his diploma in electrical engineering from Darmstadt Technical University in 1971, and joined Siemens the same year. Since 1975 he has been engaged in research and development of electron-optical systems for the production and testing of integrated circuits. This includes e-beam projection, e-beam writing, and e-beam testing.

Matthias Brunner *Siemens Research Laboratories, Otto Hahn Ring 6, D8000 Munich, Federal Republic of Germany.* Dr. Brunner has a diploma in physics; he received a Ph.D. from the Technical University of Berlin in 1981 for his investigations on electron diffraction and scattering. From 1981 to 1983, during postdoctoral employment at the IBM Thomas J. Watson Research Center, he worked on electron-beam testing. Dr. Brunner joined Siemens in 1984 to continue his work in electron-beam technologies. Between 1985 and 1988 he was responsible for SEM analytics and the development of new e-beam metrology and inspection techniques. Currently his activities focus on the testing of fast integrated circuits as well as e-beam testing of bare circuit boards. Dr. Brunner is a member of the ITG committee for contactless testing of electron components.

Burkhard Lischke *Siemens Research Laboratories, Otto Hahn Ring 6, D8000 Munich, Federal Republic of Germany.* Prof. Lischke was educated at the Technical University of Berlin, where he received his Ph.D. in 1971. He was awarded the Scheel Prize of the Berlin Physical Society for his research work on the structure of the flux quantum in superconductors. His subsequent research on magnetic domains and current distribution in superconductors led to the development of vortex and decoration microscopy. In 1974 Prof. Lischke joined the Siemens Instrumentation Plant Berlin, where he developed an e-beam stepper for lithography. In 1979 he was appointed a professor at the Technical University of Berlin. The same year he moved to the Corporate Research and Development Laboratory of Siemens in Munich, where he started research work in the fields of high-speed e-beam probing of integrated circuits, nano-metrology of small patterns, e-beam testing of printed circuit boards, and e-beam lithography, relating both to applications and instrumentation development. Prof. Lischke is currently responsible for e-beam technology in the department of solid-state electronics at Siemens.